Master's Thesis of Park Hyeon-kyu

Information processing duplex based on spin-waves by micromagnetics simulation

미소자기 시뮬레이션을 통한 스핀파 기반
정보처리 듀플렉스 시스템 연구

February 2018

Graduate School of Engineering
Seoul National University
Material Science and Engineering Major

Park Hyeon-kyu

Information processing duplex based on spin-waves by micromagnetics simulation

Name of Examiner

Submitting a master's thesis of Public Administration

February 2018

Graduate School of Engineering

Seoul National University

Material Science and Engineering Major

Park Hyeon-kyu

Confirming the master's thesis written by

Park Hyeon-kyu

February 2018

Chair _____(Seal)

Vice Chair _____(Seal)

Examiner _____(Seal)

Abstract

Duplexer is the electronic device that allows the bi-directional (duplex) communication between the receiver and the transmitter. It is also one of the circulator-derivatives whose recent research subject is size miniaturization. Spin-waves are emergent information carrier with GHz-frequency and non-Joule heating dissipation. In spin-wave circuits, the magnetic nonuniformities as well as change in wave vector make the path of spin-wave improbable. In this study, the model structure of spin-wave duplexer is proposed and studied by micromagnetics simulation, which have provided the realistic modelling of spin dynamics in numerous spin-wave studies. Combined with the halfvortex, which is the topological structure formed at the edge of magnetic film, the proposed model structure is able to guide the spin-wave in a robust and reproducible way.

Keyword : duplexer, micromagnetics simulation, halfvortex

Student Number : 2015-20822

Table of Contents

Chapter 1. Introduction

1.1. Research Background

It is known that the progress in electronics is tackled by many issues, which entail heat dissipation from a lot of origins. As faced by these issues, various intelligent schemes, for example, utilization of photon [1], phonon [2], and magnetic moment of electrons [3-7], have been proposed as resolution. Among them, using the magnetic moment of electrons is prominent, in terms of frequency regime (from ~0.1 to ~10^2 GHz), non-Joule heating dissipation, and easy controllability owing to its dispersive character [8,9]. The idea of exploiting collective excitation of the magnetic moment (spin-wave) had been mooted for a long time [3], but its experimental demonstration took more than a score of years alongside the advent of low-damping magnetic materials [10-12], realistic micromagnetics simulation [13-15], and state-of-the-art measurement techniques [16,17].

In the last decades, control of magnetic topological defects (vortex, domain wall, skyrmion, etc.) has been explored [18-20] to operate magnetic devices at low energy costs [21,22]. The magnetic topological defects are robust and unremoved by the local turbulence, and this point makes them affect spin-waves reproducibly [23-28]. In what is following, we will see that presence of topological structure (Figure 1.1) in our proposed

model structure leads to the deflection of spin-wave in a certain way. Although the researches immediately about the interaction between spin-wave and halfvortex are limited [18,73], it can be deduced from the previous researches about the effect of spin textures on spin-waves that the presence of halfvortex affects the spin-wave propagation.

Recently, the attention toward circulator-derivatives (duplexer, isolator, reflex amplifier, etc.) has increased [85-88]. In the thesis, the magnetic structure which enables spin-wave to communicate bi-directionally (duplex) is proposed and studied with aid of micromagnetics simulation. The micromagnetics simulation claims to accurately simulate the real spin dynamics [13,14] and has already proven the realistic simulation of the magnetic behaviors in numerous cases [46,58,59].

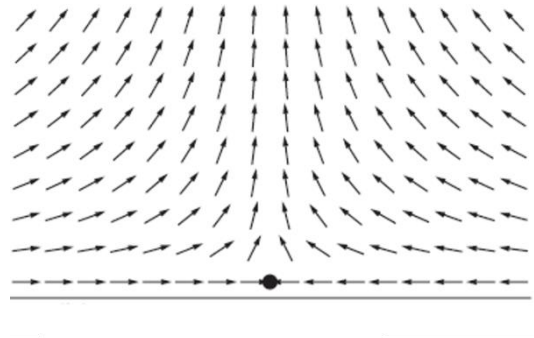

Figure 1.1. Schematic configuration of magnetic halfvortex [18]

1.2. Background Concepts

1.2.1. Magnetic topological defects

The magnetization state of magnetic films is sometimes more energetically stable by containing topological defects [29,30]. In the last decades, the intense attention paid to the magnetic topological defects has led to a plethora of researches [18-28]. For example, the low energy cost of switching vortex states suggests their application in spin-based memory and logic devices [21,22].

Theorists [29,30,32] explain the magnetic topological defects in terms of order parameter. The order parameter defines the degree of order in materials where the magnetic topological defects shall exist. The theories based on order parameters leave the magnetic topological defects with integer or half-integer charges [33].

The magnetic topological defects typically have the singular core at which the magnetization is singular. They are classified by the position of this singular core into bulk defects and edge defects. Bulk defects have the singular core inside of the material, whereas edge defects have the singular core outside of the material. In fact, the edge defect have its singular core outside of the material by a certain quantity called "effective magnetic length" (Figure 1.2 (c)),

$$\Lambda = 4\pi\lambda^2/t\log(w/t)$$

($\lambda = (2A/\mu_0 M_S^2)^{1/2}$: exchange length, *w*: film width, *t*: film thickness), which holds in the narrow magnetic films [18,73]. That

is, the core position and hence the configuration of halfvortex depend on the material parameters like exchange constant (A) and saturation magnetization (M_S).

The bulk defects and the edge defects are again classified according to their "topological charge" (winding number). The definitions of topological charge [18,73] each give vortex, antivortex, and halfvortex the charge of +1, -1, and +1/2 or -1/2. These definitions lead to the conservation law of topological charge. The net topological charge is conserved by 1-g in a flat nanomagnets with g holes,

$$\sum_{\text{edge}} n + \sum_{\text{bulk}} n = 1 - g.$$

(n: topological charge). For example, the hole-less nanomagnet can have two +1/2-charged halfvortices at the opposite ends, or a +1-charged vortex in the center (Figure 1.3) [18,34]. The conservation law also explains the dynamic transformations of topological defects [19-22,35].

1.2.2. Magnetic nonuniformities

To implement spin-waves in circuits, the uniformity of circuit material's magnetic properties should be considered. Spin-wave has mode characteristics that depend on the local variations in magnetic properties like magnetization, effective field, and anisotropy coefficient [3,36-47]. Therefore, spin-wave modes in circuit are only intact when the local magnetization and effective

field that spin-wave sees on its track are uniform.

The uniform magnetization is the energetically stable state for magnetic wires, but the uniform effective field is hard to achieve and depends on geometric factors like curvature of circuit [46]. The possible solutions can be considered by use of materials with perpendicular magnetization anisotropy (PMA) [47,92], local generation of magnetic field [91] and use of strip-domain wall as spin-wave channel [92].

The effects of magnetic nonuniformities in spin-wave circuits are summarized by three points.

1. The nonuniform dipolar field and anisotropy coefficient are relevant to spin-wave deflection. The equation of spin-wave motion resembles Schrödinger equation [48,49], and the scalar potential counterpart in the spin-wave equation explains the deflected spin-wave trajectory (as if the electrons are scattered by the potential barrier) [40-42,44] (Figure 1.4 (a)).
2. The nonuniform magnetization and DMI (Dzyaloshinskii-Moriya interaction) constant are relevant to specific phenomena [26-28,50]. They are the origin of the vector potential counterpart in the spin-wave equation, so the related phenomena (Aharonov-Bohm effect, Lorentz force) are also found for spin-waves [27,28,50-53] (Figure 1.4 (b)).
3. The nonuniform magnetization also leads to the additional damping [54], which may affect the switching time of magnetic elements [55]. The damping term has the magnitude proportional to the fourth-power of spin-wave amplitude.

The magnetic nonuniformities in topological defects (skyrmion, Bloch point, domain wall) also control spin-wave, but they will simultaneously suffer back from the momentum of spin-wave [23-28,56,57]. The isolated halfvortex can be expected to affect spin-wave, but it is rarely mentioned in room-temperature experiments [39,41].

1.2.3. Duplexer

Spin-wave researches over the past years have proposed alternatives for traditional electronics [22,91,92]; they range from spin-wave logic gate, spin-wave filter, spin-wave splitter, spin-wave multiplexer, and so on.

Recently, three-port devices derived from circulator (e.g. isolator, duplexer, reflex amplifier) have been studied to miniaturize their size [85-88]. Duplexer (Figure 1.5 (a)), which is a 3-port electronic device required for the bi-directional (duplex) communication, allows both the signals from the transmitting port and the receiving port to share the common antenna. Inside the duplexer, the signal from transmitting port only goes to antenna, while the signal from antenna only goes to receiving port (Figure 1.5 (b)). Thereby, the device can protect the receiver from unwanted and potentially damaging high power signals.

1.2.4. Previous three-port spin-wave systems

Different kinds of three-port spin-wave devices, which are similar in the structure, but different in mechanism and function each other, have been researched. Recent study subjects include magnonic (spin-wave) beam splitter, spin-wave multiplexer, and paved spin-wave fiber.

1. The magnonic beam splitter in [41] (Figure 1.6 (a)) is in form of a T-shaped circuit, and two different spin-wave modes (MSSW mode and BVMSW mode in [41]) are excited each in vertical and horizontal sections of the T-shaped circuit. The spin-wave modes are interconverted only when the wavenumbers of both modes are the same.
2. The spin-wave multiplexer in [91] (Figure 1.6 (b)) is in form of a Y-shaped circuit, and its spin configuration is controlled by the electrical circuit embedded beneath the spin-wave circuit, which in turn determines the trajectory of spin-wave.
3. The paved spin-wave fiber in [92] (Figure 1.6 (c)) is in form of a Y-shaped circuit, and employs the strip-domain wall as the spin-wave channel. The connectivity of the strip-domain wall between the ports determines the trajectory of spin-wave.

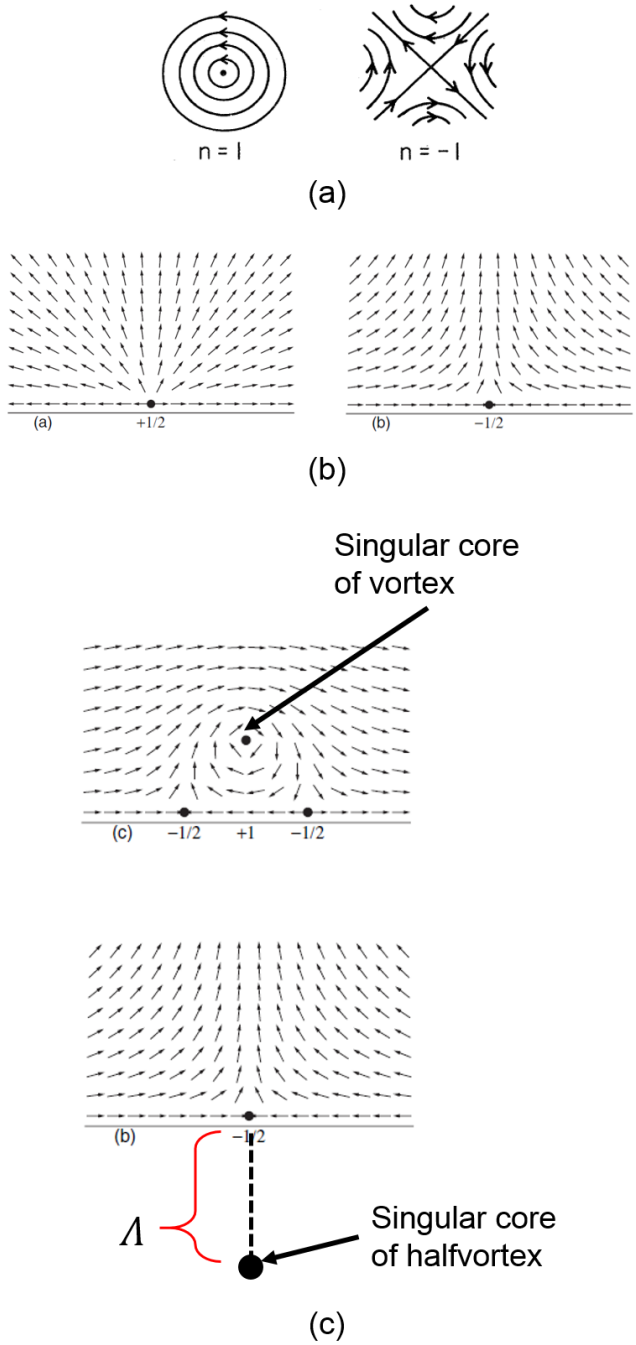

Figure 1.2 (a) Schematic configuration of vortex and antivortex, and their charges [29], (b) schematic configuration of halfvortex of two types and their charges [18,73], (c) the position of singular core of vortex (bulk defect) and halfvortex (edge defect) [18,73].

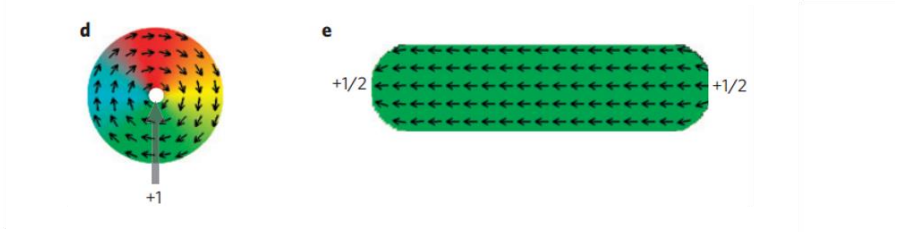

Figure 1.3 Two possibilities of topological charge distribution in a hole-less magnet ($\sum_{\text{edge}} n + \sum_{\text{bulk}} n = 1$), a vortex (+1*1=1) or halfvortices (+1/2*2=1) [34].

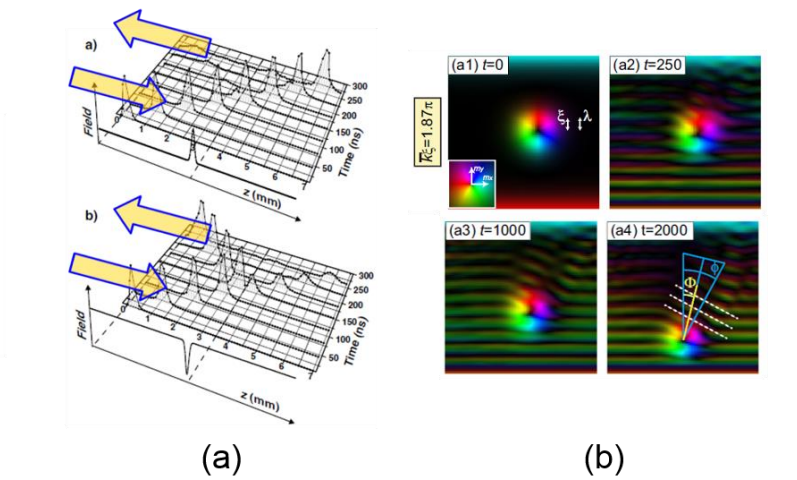

Figure 1.4 (a) Spin wave tunneling and reflection by scalar-like potential [40], (b) spin wave scattering by vector-like potential from skrymionic texture [27].

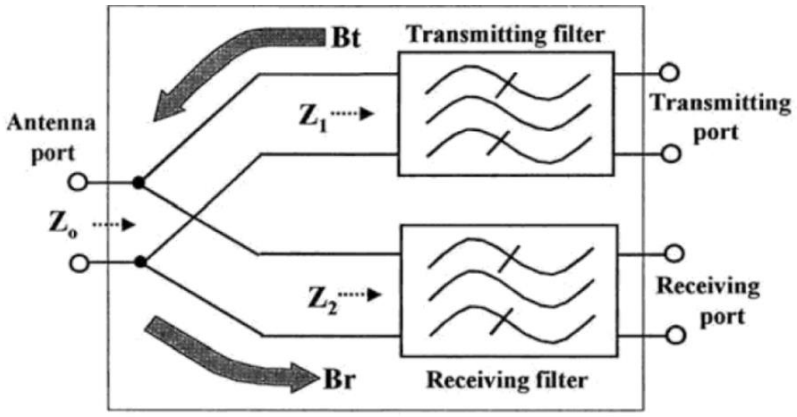

Fig.44. The structure of antenna duplexer.

(a)

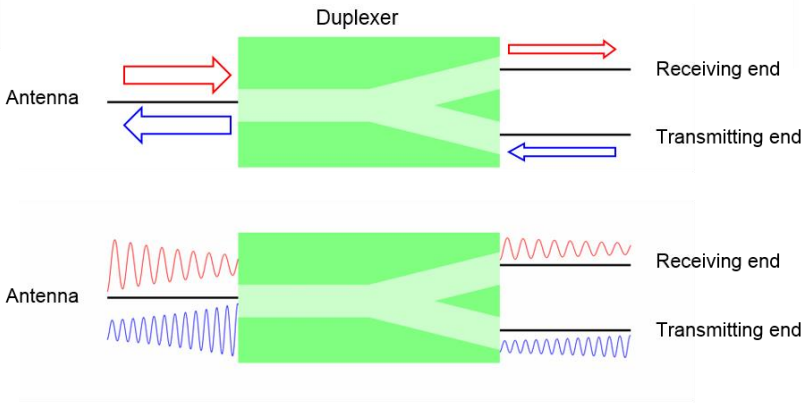

(b)

Figure 1.5 (a) Schematics of the electromagnetic duplexer [81], (b) the signal transport in duplexers (red arrow/wave: receiving signal, blue arrow/wave: tranmitting signal)

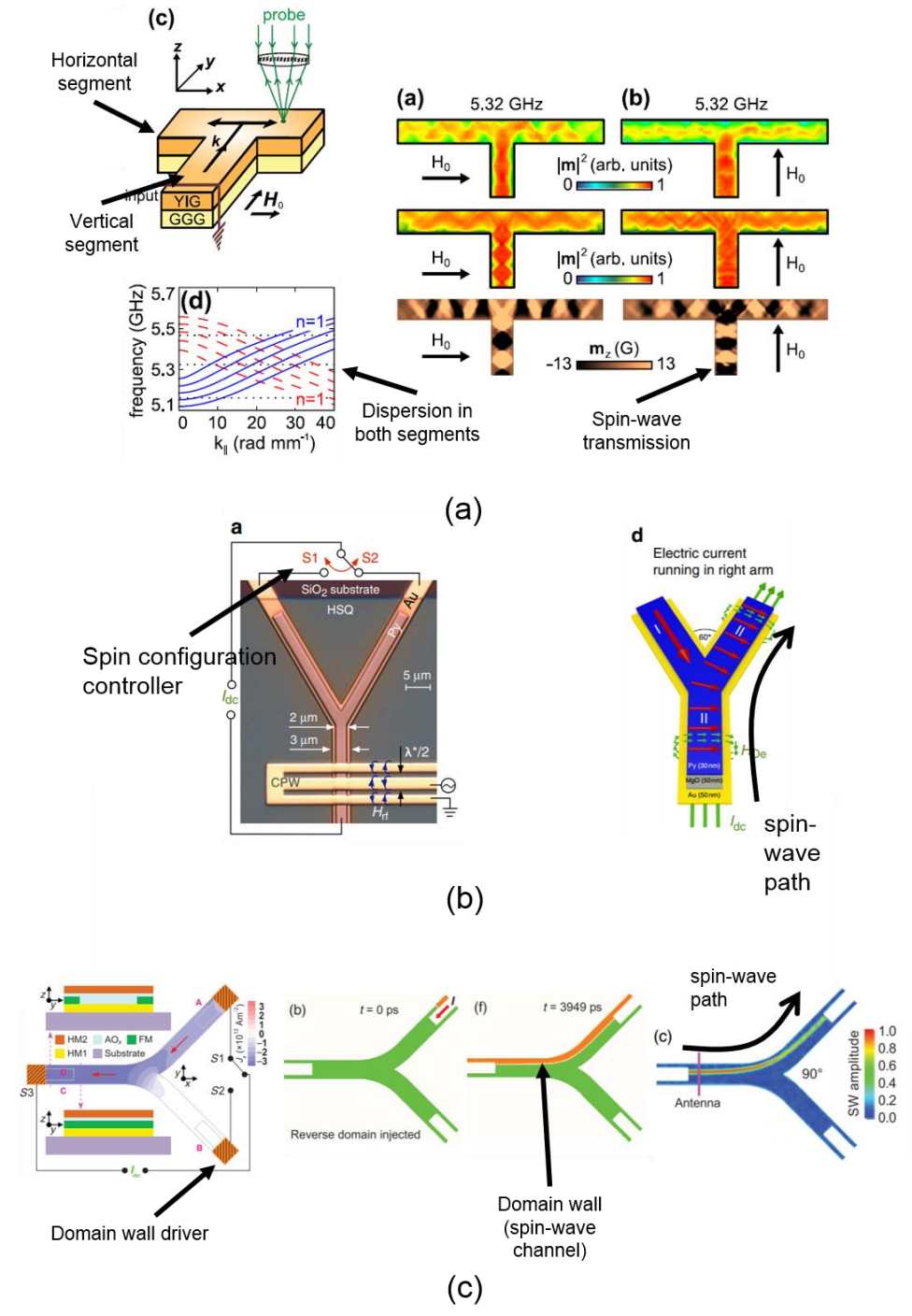

Figure 1.6 (a) Magnonic beam splitter [41], (b) spin-wave multiplexer [91], (c) spin-wave fiber [92]

1.3. Outline of thesis

In the thesis we will see the magnetic structure that functions like a three-port spin-wave duplexer in which the spin-wave path entirely relies on the halfvortex-configuration inside the structure. The details of simulation and the magnetic structure are in Chapter 2, the simulation results will be presented in Chapter 3, and the thesis will be concluded in Chapter 4.

Chapter 2. Research Method

2.1. Micromagnetics simulation

2.1.1. Problem of micromagnetics

Micromagnetics is the computational method that predicts the magnetic behaviors and supplements experimental results in sub-micrometer length scales. The merit of using micromagnetics is that when joined with Fourier transform [46] and dynamical matrix method [58,59], the spectral behavior of spin-wave in a range of frequencies is displayed at once.

There are two types of micromagnetics problems:

1. *Calculate the ground configuration* by minimizing the magnetic energy,

$$E[\vec{M}] = E_{\text{exch}} + E_{\text{dipolar}} + E_{\text{ext}} + E_{\text{etc.}},$$

in which

$$E_{\text{exch}} = A \int \left|\vec{\nabla} M_x\right|^2 + \left|\vec{\nabla} M_y\right|^2 + \left|\vec{\nabla} M_z\right|^2 dV ,$$

$$E_{\text{dipolar}} = -\frac{\mu_0}{2} \int \vec{M} \cdot \vec{H}_{\text{dipolar}} dV ,$$

$$E_{\text{ext}} = -\mu_0 \int \vec{M} \cdot \vec{H}_{\text{ext}} dV ,$$

(A: exchange stiffness, $\vec{H}_{\text{ext}}$: external magnetic field) and the $E_{\text{etc.}}$ includes other contributions to the energy like anisotropy of crystal structure and Dzyaloshinskii-Moryia

interaction (DMI).

2. *Calculate the spin dynamics* by solving Landau-Lifshitz-Gilbert (LLG) equation

$$\frac{d\vec{M}}{dt} = -\gamma\vec{M} \times \vec{H}_{\text{eff}} + \frac{\vec{M}}{M_{\text{S}}} \times \alpha \frac{d\vec{M}}{dt}$$

Each term on the right accounts for precession and damping of spin. In fact, the effective field $\vec{H}_{\text{eff}}$ is the functional derivative of the magnetic energy density with respective to the magnetization.

Because the analytical solutions for LLG equations are only available for a limited number of systems, solving general problems requires use of micromagnetics simulation packages. The commonly used packages are magnum.fe, OOMMF, and Mumax [69-71].

2.1.2. Two types of micromagnetics simulation packages

There are two types of micromagnetics simulation packages, according to their method to evaluate the dipolar field [60].

1. The first type of packages (FEMME, magnum.fe) solve the magnetic Gauss's law on discretized domains (V) [61,62],

$$\nabla^2\phi = \begin{cases} \vec{\nabla} \cdot \vec{M}, & \text{in } V \\ 0, & \text{outside } V \end{cases}$$

$$\phi^{\text{outside}} = \phi^{\text{inside}}, \qquad \text{on } \partial V$$

$$\left(\frac{\partial\phi}{\partial n}\right)^{\text{outside}} = \left(\frac{\partial\phi}{\partial n}\right)^{\text{inside}} - \vec{M} \cdot \hat{n}, \qquad \text{on } \partial V$$

($\vec{H}_{\text{dipolar}} = -\vec{\nabla}\phi$) in which ϕ is magnetic scalar potential, and discretization is whether finite difference mesh (FD mesh) or finite element mesh (FE mesh) consisting of discrete polygonal subdomains.

The problem of solving above equation is lack of the boundary condition in exterior of material; it was hypothesized that the proper calculation requires the meshing to be extended over the material surface as thick as five times the size of material [63]. To overcome this difficulty, various techniques have been proposed:

a. *to reduce the size of the external mesh*, using an asymptotic boundary condition [64] and mapping of exterior domain into parallelepiped shells [61,65].
b. *to avoid a discretization of the exterior space*, by use of hybrid FE/BE (finite element-boundary element) methods [62].

2. The second type of packages (OOMMF, Mumax) make use of the Green function solution of above problem [66-68],

$$\vec{H}_{\text{dipolar}} = \int \vec{\nabla}_r \vec{\nabla}_{r'} \frac{1}{|\vec{r}' - \vec{r}|} \cdot \vec{M}(\vec{r}')dV' ,$$

which is numerically evaluated by using fast Fourier transform (FFT). However, evaluation by fast Fourier transform requires the uniform Cartesian grid as the FD mesh. The material surface in this method is approximated along the grid lines in the shape of a staircase. Such approximation is only appropriate for rectangular-shape materials and only there, the

boundary conditions ($\partial\vec{M}/\partial\hat{n} = 0,\ \partial\phi/\partial\hat{n} = 0$) are evaluated correctly [60] (Figure 2.1).

2.1.3. Finite Element MicroMagnEtics (FEMME)

For accurate calculation in curved magnetic structure, the finite element (FE) method software should be employed. Finite Element MicroMagnEtics (FEMME) package implements the preconditioned time integration, hybrid FE/BE method, nudged elastic band method, and finite temperature simulation[1]. Basic procedures of using FEMME are described in the manual. The results of simulation are visualized by any linear interpolation software programs (Paraview, MATLAB, etc.).

2.1.4. Ring-down method

Ring-down method [69,70] is employed to efficiently determine the spin-wave spectral behavior, providing reliable solutions comparable to eigenvalue calculation [71]. The method is comprised of three steps:

1. *Find the equilibrium magnetization state*, often starting from a trial high-energy state. The robust way to find the stable state is free relaxation, which is the relaxation with raised damping parameter. Also available is the conjugate gradient method

[1] FEMME webpage (http://suessco.com/simulations/solutions/femme-software/)

supported in some packages, which however tends to fail on very high energy states [72].

2. *Apply a short-lived and sufficiently weak field*. In fact, the resultant excitation consists of spin-wave components each oscillating at different frequencies.[2]
3. *Analyze the spin-wave components by performing FFT*. In what is following, the stable magnetization lies within the film. Then we can make use of the M_z component as the spin-wave excitation. The spin-wave component at each frequency is calculated from [69]

$$S_z(\vec{r}, f) = |F_z(\vec{r}, f)|^2,$$

$$F_z(\vec{r}, f) = \sum_{k=1}^{N} M_z(\vec{r}, t_k) e^{-2\pi i f t_k}$$

(N: time step number), in which M_z is numerical magnetization data at predefined grids.

[2] The LLG equation is sum of equations on the single-frequency (monochromatic) spin-wave ($\vec{m}(\vec{r}, t) \sim e^{i\omega t}$) oscillating at ω. With negligible amplitude of spin-wave it is in form of

$$\frac{d\vec{m}}{dt} = -\gamma\left(\vec{m} \times \vec{H}_0 + \vec{M}_0 \times \vec{h}\right) \sim e^{i\omega t}$$

($\vec{M}_0(\vec{r})$: an equilibrium configuration, $\vec{H}_0(\vec{r}) = \vec{H}_{\text{eff}}[\vec{M}_0(\vec{r})]$, $\vec{m}(\vec{r}, t) = \vec{M}(\vec{r}, t) - \vec{M}_0(\vec{r})$, $\vec{h}(\vec{r}, \mathrm{t}) = \vec{H}_{\text{eff}}(\vec{r}, t) - \vec{H}_0(\vec{r})$), in which the equilibrium condition $\vec{M}_0(\vec{r}) \times \vec{H}_{\text{eff}}[\vec{M}_0(\vec{r})] = 0$, and the second-order term ($\vec{m} \times \vec{h}$) and the damping term are negligible,

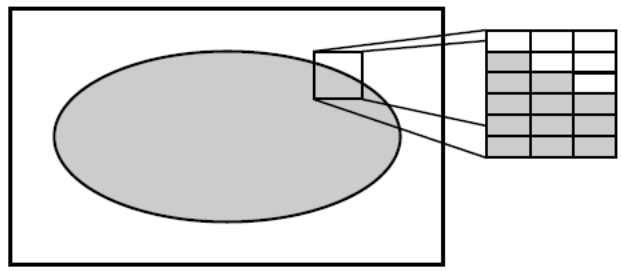

Fig. 2. Staircase approximation: the irregular cells near the boundary have been replaced by rectangles.

Figure 2.1. Staircase approximation for a curved boundary [60]

2.2. Proposal of spin-wave duplexing system

2.2.1. Geometry and material parameters

The model system proposed for spin-wave duplexer is comprised of three magnetic nanowires (MNWs) in triple symmetry and a ring at the center (Figure 2.2 (a)). Both MNWs and the ring have the width w=50nm and thickness t=10nm. Simulation parameter of bulk Permalloy (Py, $Ni_{0.8}Fe_{0.2}$) is used, also recognizing that a few tens of nanometer is considered thick for Py to involve nano-effects [76].

The geometrical dimensions are larger than the exchange length,

$$\lambda = (2A/\mu_0 M_S)^{1/2}$$

(A: exchange stiffness, μ_0: vacuum permeability, M_S: saturation magnetization), which is 5.29 nm for Permalloy. The exchange length has two meanings. First, it represents the minimum size of magnetic particle that assures the uniform magnetization reversal [93]. Second, its square number is directly proportional to the exchange interaction strength. This enables exchange-dominated spin-waves to have the wavelength proportional to the exchange length.

In the micromagnetics simulation, the numerical data of magnetization is interpolated on tetrahedral meshes, so the size of meshes should be under the exchange length for more accurate calculation results. The smallest wavelength of spin-wave excited in the following simulation is about λ_{min}=25nm at the Nyquist

frequency 50GHz, well exceeding the exchange length. Keeping this, the size of tetrahedral mesh used in the simulation is set to range around double of the exchange length (Figure 2.2 (b)).

Also, it is assumed that no spin-wave is excited in the thickness direction because the wavelength in this direction should be less than 10nm, which is much lower than λ_{min}.

2.2.2. Possible ground states

Stable magnetization state in MNWs tends to direct in the axial direction in order to minimize the surface magnetic charge (shape anisotropy). This should allow 16 spin configurations (2*2*2*2=16) in the proposed model system (Figure 2.3), but considering the three-fold symmetry of the structure of the model, only 4 configurations are distinguishable. Further, the manipulation of the LLG equation shows that spin-wave excitations in the inverse magnetization configuration ($-\vec{M}_0(\vec{r})$ and $\vec{M}_0(\vec{r})$) rotate in the opposite direction but equal in magnitude. Therefore, the consideration of only two spin configurations (model A, B) is enough in the simulation; model A has inward magnetization in all the MNWs and counter-clockwise magnetization in the ring, while model B has inward magnetization in one of the MNWs, outward magnetization in the other MNWs, and counter-clockwise magnetization in the ring.

2.2.3. Halfvortices in the model system

Because the model structure bears a hole, the net topological charges of all the defects present in the structure should sum to 1-1=0. First, the halfvortices with positive charge +1/2 necessarily exist at each end of the MNWs. This leaves the missing charge of -3/2. Second, three halfvortices with negative charges of -1/2 exist in the ring, but their distribution depends on the spin configuration of the MNWs. For model A, the distribution of -1/2-halfvortices are symmetric, while for model B, the distribution is asymmetric (Figure 2.4 (a)). It is found from calculation that demagnetizing field around the halfvortices is nonuniform (Figure 2.4 (b)), and therefore presence of halfvortices will result in not only the nonuniform magnetization but also the nonuniform effective field.

2.2.4. Exciting spin-waves in the system

As the procedure of ring-down method, the ground magnetization state is firstly found from free relaxation. Secondly, the spin-wave is excited at the edge of MNWs by a sine-cardinal function (Figure 2.5 (a)),

$$\vec{H} = H_0 \frac{\sin 2\pi f(t - t_0)}{2\pi f(t - t_0)} \hat{x},$$

(H_0=100Oe, f=50GHz, t_0=0.1ns, $\hat{x}$: in transverse direction of the MNW). The excitation of spin-wave at the edge of one of the MNWs will represent the inflow of spin-wave into that MNW. To simulate the inflow of spin-wave into all the MNWs, the spin-

wave is repeatedly excited at all three edges of the MNWs. However, as for model A, it is enough to excite the spin-wave at the edge of only one MNW since the magnetization and the effective field in model A is in triple symmetry.

Total simulation time of 10 ns and time discretization of 0.01 ns are used, resulting in frequency resolution of 0.1 GHz and Nyquist frequency of 50 GHz. The smallest wavelength in the simulation is about 25nm at 50GHz, well covering the typical size of tetrahedral meshes (5nm).

As the external magnetic field is applied on the edge of MNWs, the spin-wave is excited all over the model structure (Figure 2.5 (b)). By Fourier transform the spin-wave contribution at specific frequency can be extracted (ring-down method), and from the data of spin-wave contribution we can predict where the imported spin-wave of specific frequency will propagate.

In fact, the spin-wave data at each frequency is composed of 39440(number of nodes)*1001(number of time steps)=4000000 numbers. Rather than showing all these data time by time, it is sufficient to show the Fourier transform data at given frequency (Figure 2.5 (c)) which is double of the sinusoidal spin-wave amplitude. The spatial Fourier transform data at each frequency can be visualized by using interpolation tools (Paraview, Matlab).

Further, instead of showing the spatial spin-wave data at all the frequencies, the spatial Fourier transform at each frequency can be summarized by taking the Fourier transform data along the lines that penetrate the center of cross-section of MNWs and ring

(Figure 2.5 (d)). Now the Fourier transform data at each frequency is presented in a 1*N row data (N: number of grids along the penetrating line), and the whole data over all the frequencies (number of frequency step is 501) will be in a 501*N matrix data. Such matrix data are obtained from five segments (Figure 2.6) that represents the spin-wave transmission in MNWs and ring; the MNW where the spin-wave flows in, the other MNWs where the spin-wave flows out, and the segments of the ring that connects between the MNWs.

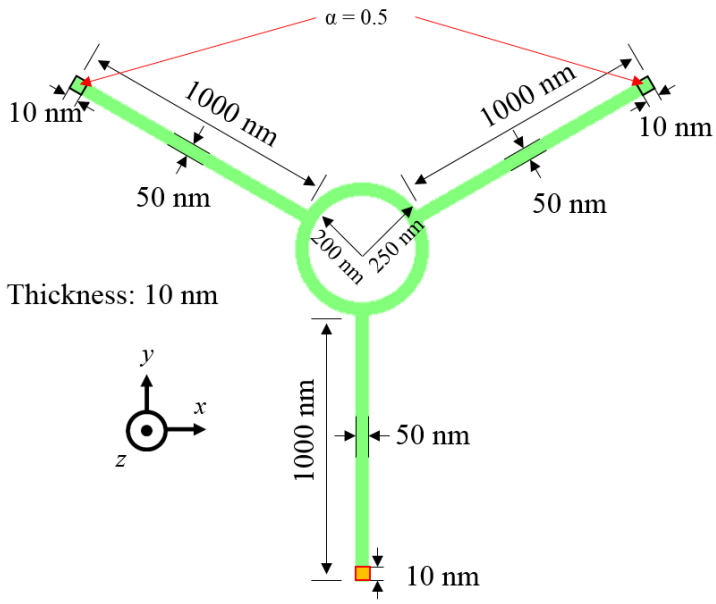

(a)

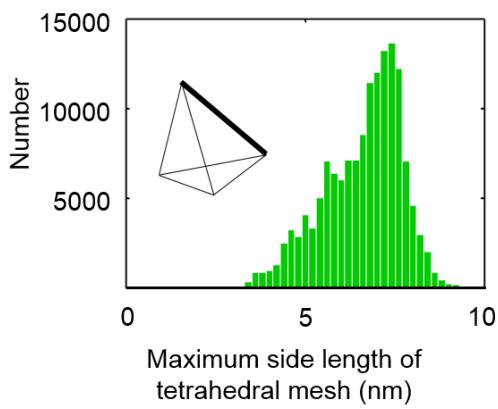

(b)

Figure 2.2 (a) The geometry of model system, (b) the distribution of mesh sizes

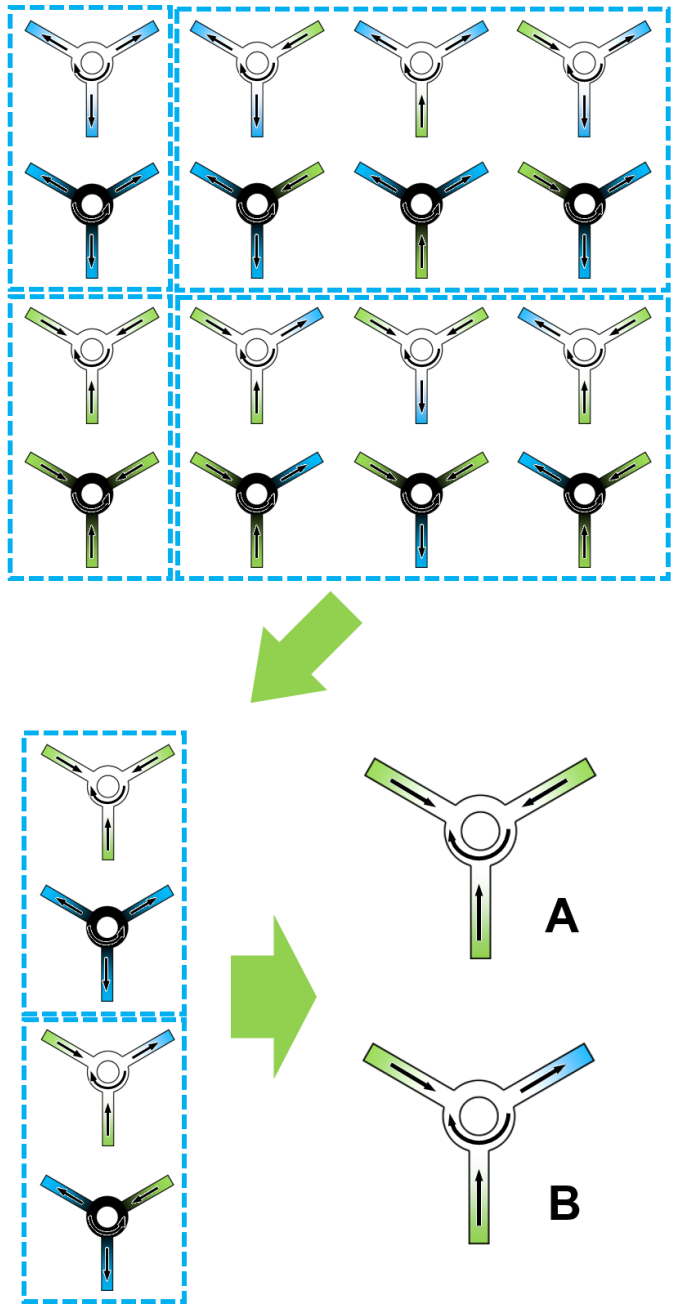

Figure 2.3 16 spin configurations are all possible for the model system, but only 4 of them are distinguishable due to symmetry, and only 2 of them have distinguishable solutions to LLG equation

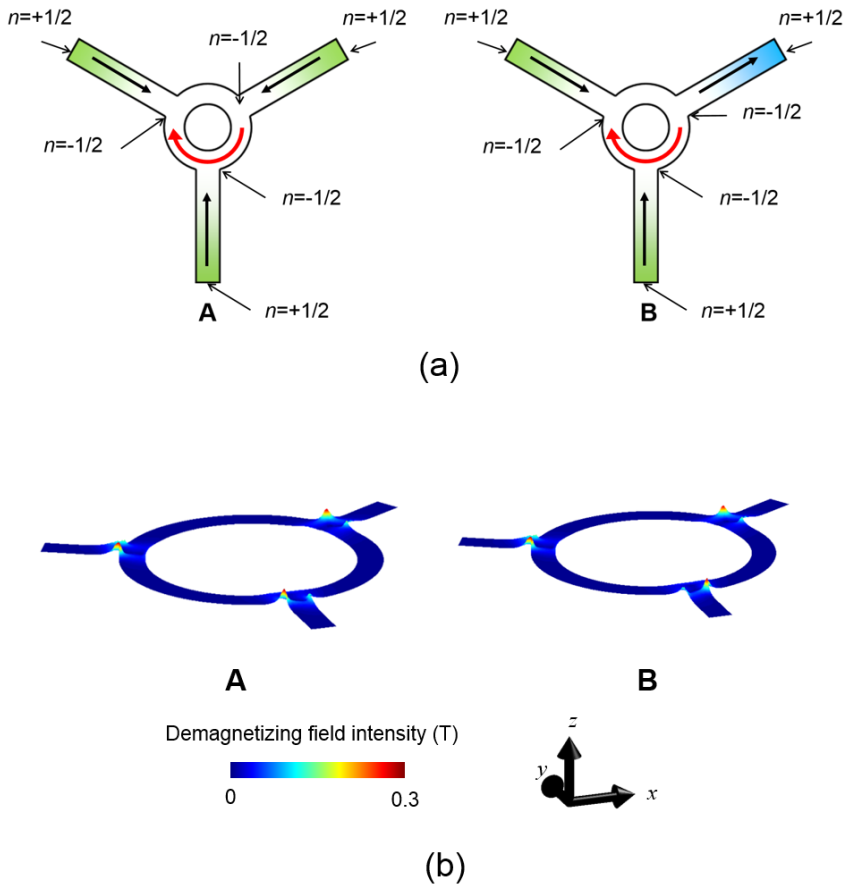

Figure 2.4 (a) Spin configuration for model system A and B, (b) intensity of demagnetizing field for model system A and B

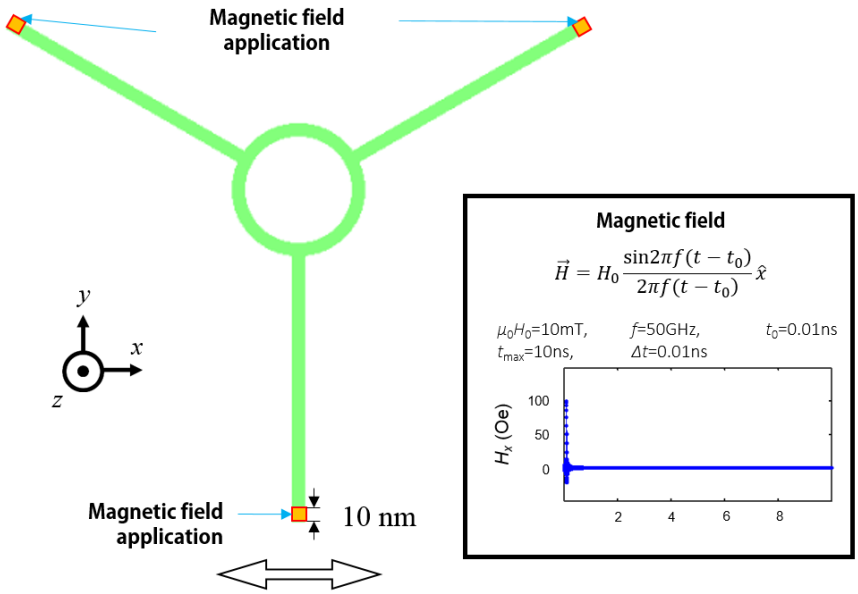
Magnetic field application
y
x
z
Magnetic field application
10 nm
Magnetic field
$\vec{H} = H_0 \frac{\sin 2\pi f(t-t_0)}{2\pi f(t-t_0)} \hat{x}$
$\mu_0 H_0$=10mT, f=50GHz, t_0=0.01ns
t_{max}=10ns, Δt=0.01ns
H_x (Oe)
100
50
0
2
4
6
8

(a)

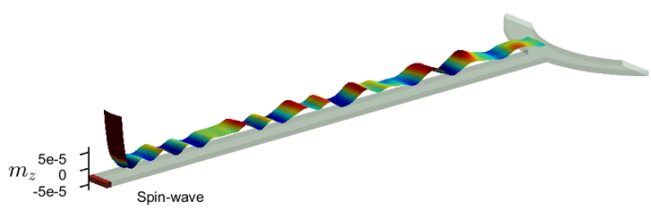
m_z
5e-5
0
-5e-5
Spin-wave

(b)

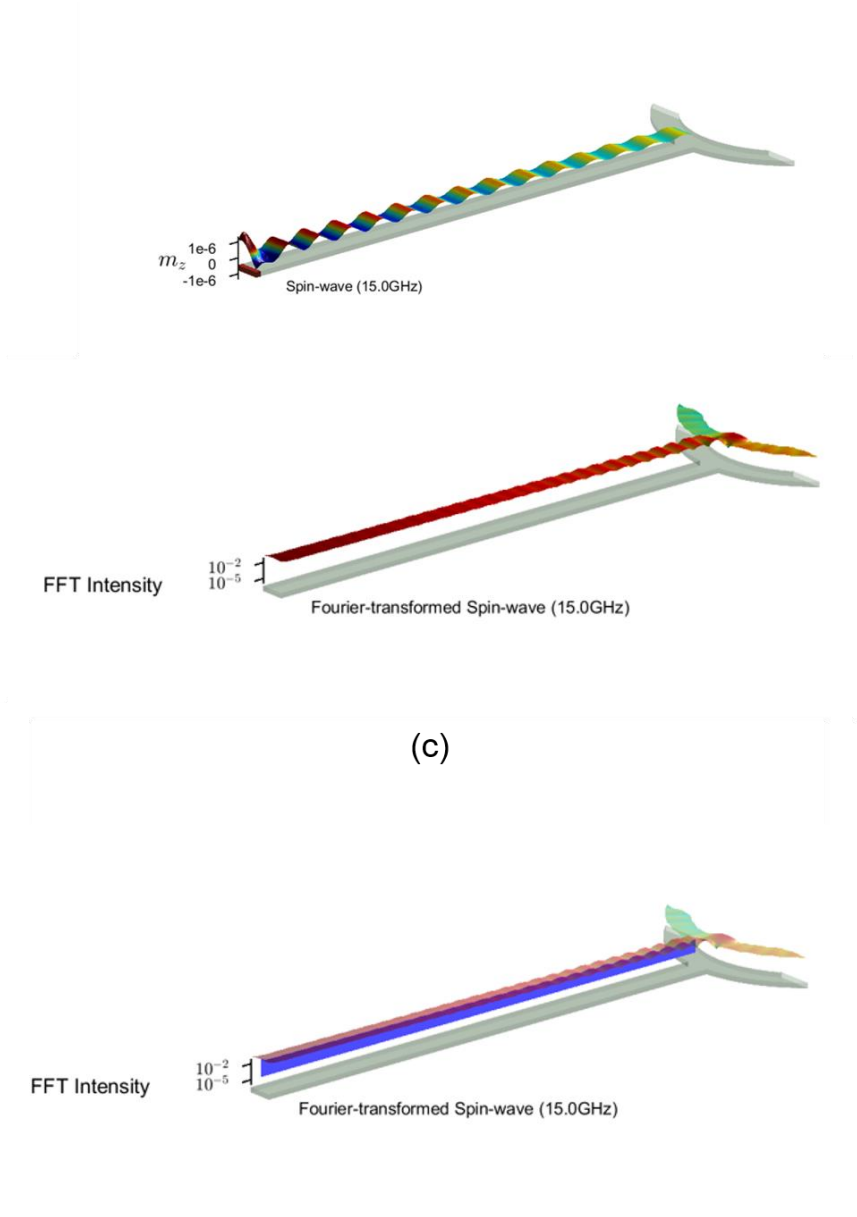

Figure 2.5 (a) Region of magnetic field application and magnetic field profile, (b) spin-wave data in time domain, (c) spin-wave data at 15 GHz in time domain and in frequency domain, (d) spin-wave data at 15 GHz in frequency domain taken at the center line

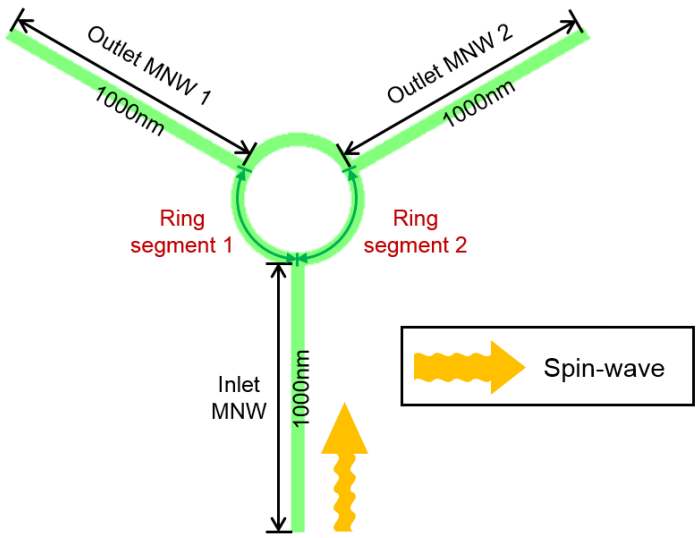

Figure 2.6 The five segments (Inlet MNW, Outlet MNW 1, Outlet MNW 2, Ring segment 1, Ring segment 2) from which the Fourier transform data is interpolated.

Chapter 3. Simulation Results

3.1. Spin-wave propagation in model system A and B

To examine the propagation behavior of spin-waves that are imported into the MNWs as well as their subsequent wave behaviors in model system A and B, the mode spectra in the frequency (f) domain were plotted along the axis penetrating the center of cross-section of the five segments (inlet MNW, outlet MNW 1, outlet MNW 2, ring segment 1, and ring segment 2) (A-Figure 3.1; B-Figure 3.2). As for the model system B, the mode spectra in f domain were obtained by exciting spin-waves at each end of three MNWs. Figure 3.2 (a1)-(e1), Figure 3.2 (a2)-(e2), and Figure 3.2 (a3)-(e3) are the mode spectra for the model system B which were obtained by spin-wave excitation at the end of bottom MNW, top-left MNW, and top-right MNW.

The mode spectra of the spin-waves injected into the inlet MNW (Figure 3.1 (a), Figure 3.2 (a1), (a2), (a3)) show a forbidden band for $f < f_{p,\,\mathrm{Py}} = 11$ GHz, the value of which corresponds to the minimum f of the spin-waves that are allowed to propagate through the Py nanowire of the given dimension. By contrast, spin-waves of $f > f_{p,\mathrm{Py}} = 11$ GHz propagate well through the entire length of the MNW and approach its end. The gap $f_{p,\mathrm{Py}}$ has an exchange-dipolar origin which can be calculated from the approximate

dispersion relation for the exchange-dipolar spin-wave [36, 89, 90] for very thin slab ($t/w \ll 1$) and cylinder ($t/w=1$). Our numerically calculated value $f_{p,\mathrm{Py}}$ = 11 GHz, with thickness t=10 nm and w=50 nm (t/w=0.2), enters between the analytically calculated values for the thin slab case (14.1 GHz) and the cylinder case (6.9 GHz).

Next, in the mode spectra of the spin-waves injected into both ring segments (Figure 3.1 (b), (d), Figure 3.2 (b1), (d1), (b2), (d2), (b3), (d3)), we find that the forward traveling spin-waves are split into both directions. This should be attributed to the nonuniform magnetization and effective field that are relevant to the complex magnetization, but the closer understanding into why the spin-wave on complex magnetization should split in that way is very complicated [39]. In [39], the whole procedure of determining the propagation direction of split spin-waves is discussed in the case of micrometer-sized magnetic structure (>5μm). Our case, with sub-micrometer dimensions, is more complicated due to limited resolution in $\vec{k}$ domain and pinning on the lateral edges that unpredictably distorts the spin-wave dispersion relation.

Finally, the spin-waves in the ring segments escape into the outlet MNWs (Figure 3.1 (c), (e), Figure 3.2 (c1), (e1), (c2), (e2), (c3), (e3)), and the splitting of spin-waves in this procedure should also be attributed to the nonuniform magnetization and the effective field.

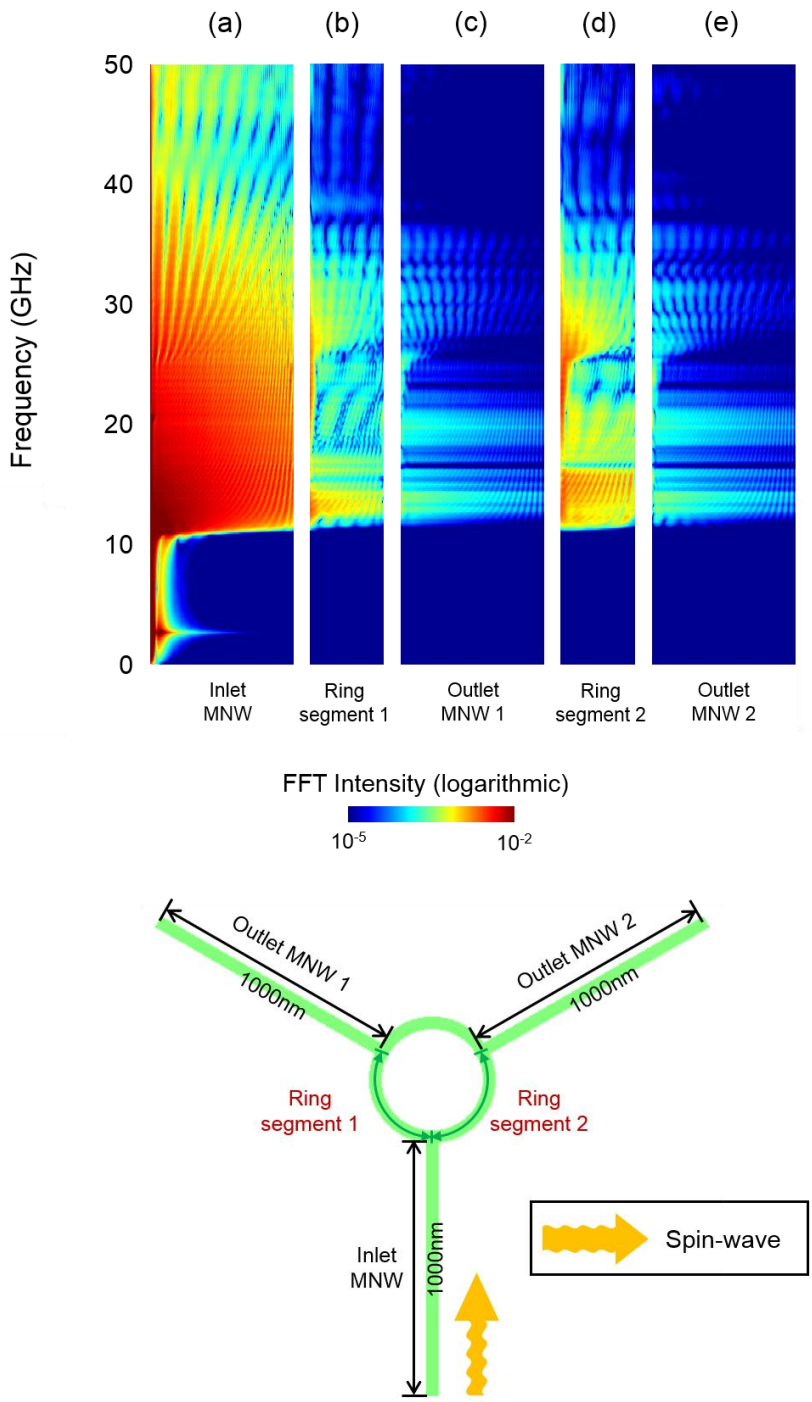

Figure 3.1 The mode spectra in *f* domain for model system A, along (a) inlet MNW, (b) ring segment 1, (c) outlet MNW 1, (d) ring segment 2, (e) outlet MNW 2

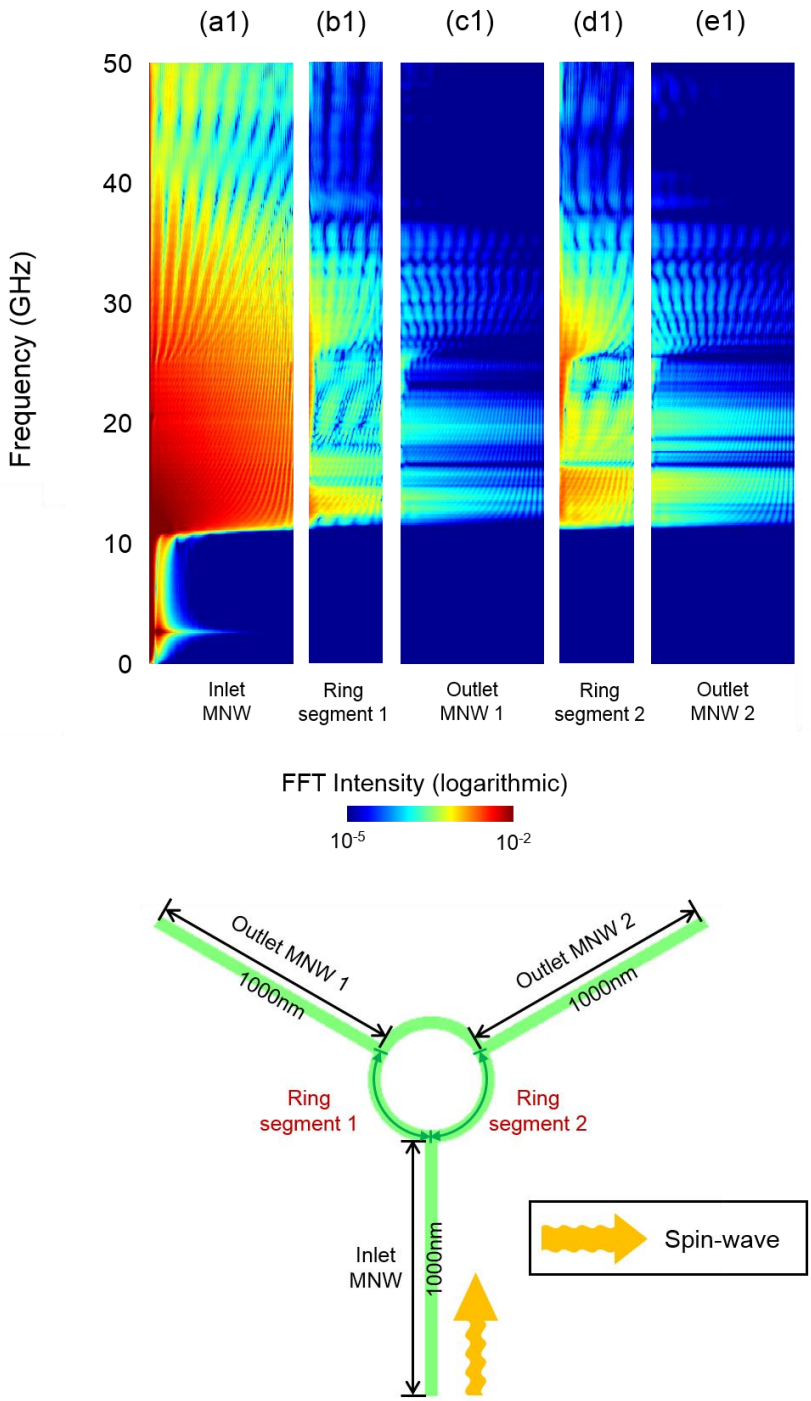
(a1)
(b1)
(c1)
(d1)
(e1)
Frequency (GHz)
50
40
30
20
10
0
Inlet MNW
Ring segment 1
Outlet MNW 1
Ring segment 2
Outlet MNW 2
FFT Intensity (logarithmic)
10-5
10-2
Outlet MNW 1
1000nm
Outlet MNW 2
1000nm
Ring segment 1
Ring segment 2
Inlet MNW
1000nm
Spin-wave

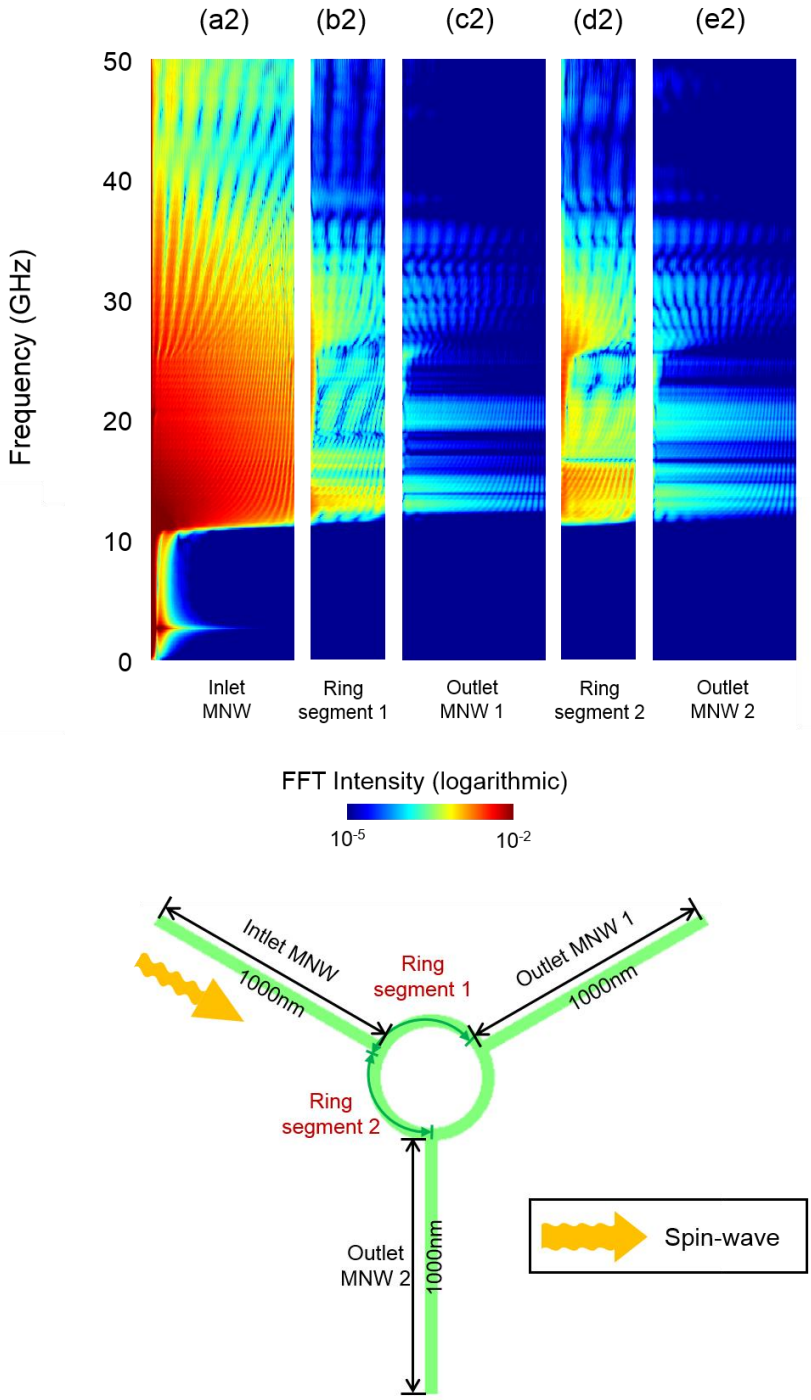
(a2)
(b2)
(c2)
(d2)
(e2)
Frequency (GHz)
50
40
30
20
10
0
Inlet MNW
Ring segment 1
Outlet MNW 1
Ring segment 2
Outlet MNW 2
FFT Intensity (logarithmic)
10-5
10-2
Intlet MNW
1000nm
Ring segment 1
Outlet MNW 1
1000nm
Ring segment 2
Outlet MNW 2
1000nm
Spin-wave

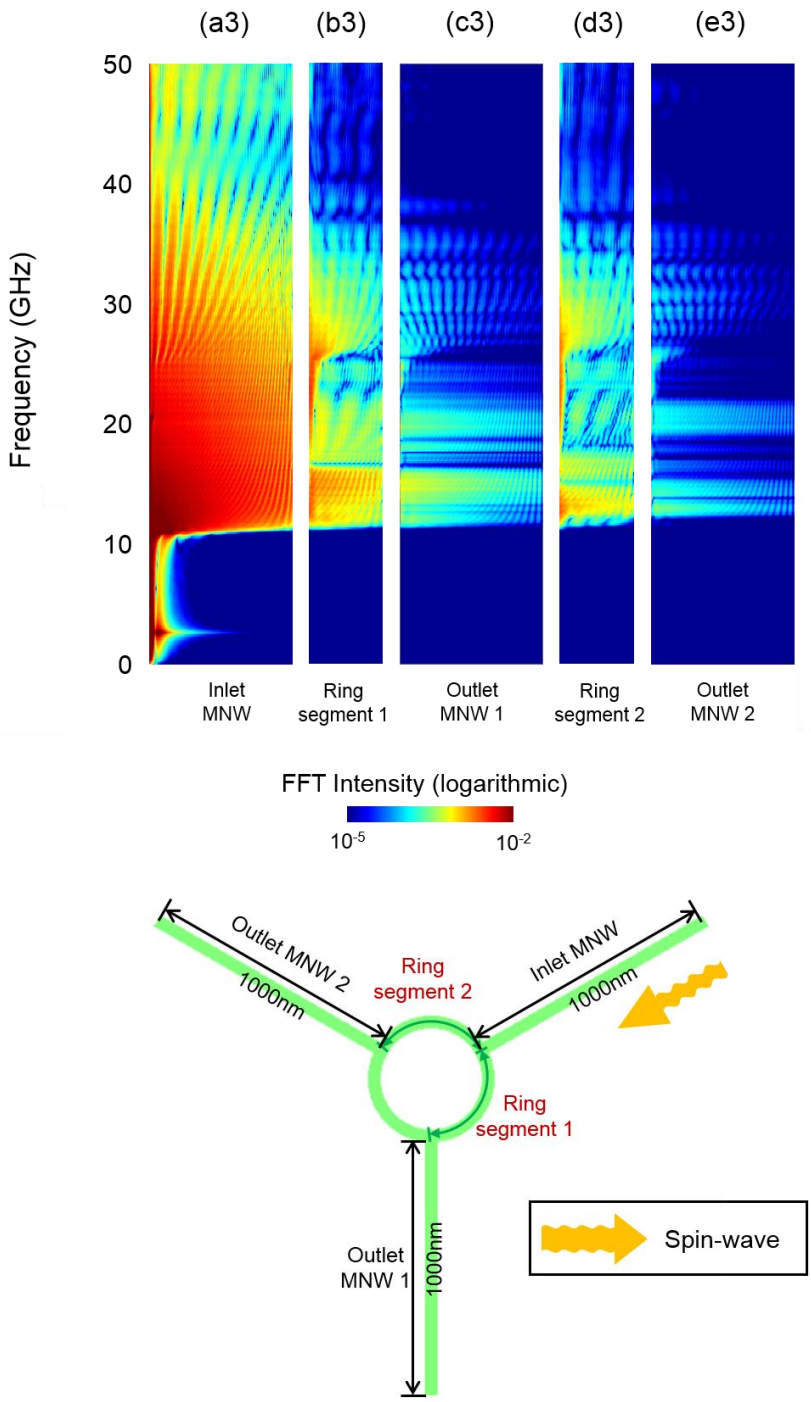

Figure 3.2 The mode spectra in *f* domain for model system B, along (a) inlet MNW, (b) ring segment 1, (c) outlet MNW 1, (d) ring segment 2, (e) outlet MNW 2.

3.2. Spin-wave dispersion in model system A and B

The ripple patterns in the mode spectra imply that the spin-waves were reflected backwards from the end and subsequently combined with the forward traveling spin-waves. To see the reflection of forward spin-waves, the dispersion relations for model system B are shown in Figure 3.3 (a)-(e) in the case of exciting spin-waves at the edge of bottom MNW. These contour graphs show the strong dispersion between f and k_l, the longitudinal component of the spin-wave wave vector $\vec{k} = (k_l, k_t)$ for the spin-waves traveling within the MNWs and the ring segments (k_t is the transverse component of the wave vector). The cases $k_l > 0$ and $k_l < 0$ correspond to the forward and backward spin-wave, respectively. From the dispersion relation for inlet MNW (Figure 3.3 (a)), the backward spin-wave that was reflected from the edge is now identified.

In fact, in all of the dispersion relations, three distinct modes are observed as indicated by the three different-colored circles in Figure 3.3 (a). In the region of $f > f_{p,\mathrm{Py}} = 11$ GHz, two different concave-up curves (marked as the red and green circles) appear. In [44, 46], it is shown that each concave-up curve represents the spin-wave modes which have different number of nodes in its mode profile in the width direction. For example, the inverse Fourier transform at 30.0 GHz on each concave shows mode

profiles with zero and two nodes, respectively (Figure 3.4 (a)-(b)). The flat branches in the region of $f < f_{p,\mathrm{Py}} = 11$ GHz are relevant to the localized mode at the end of MNWs [89]. The inverse Fourier transform at 2.6 GHz demonstrates the edge-localized mode (Figure 3.4 (c)).

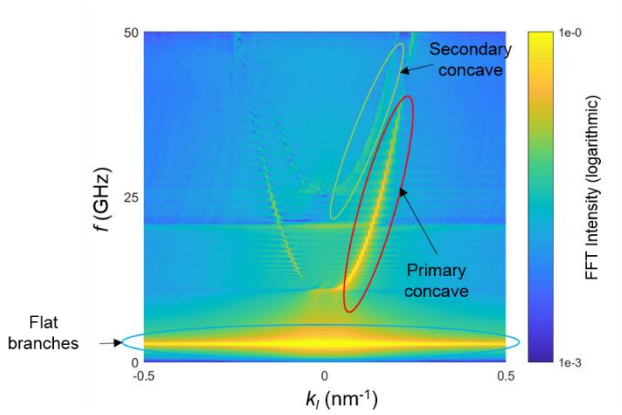

(a)

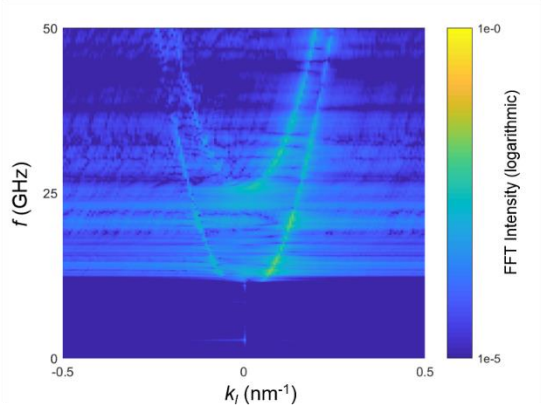

(b)

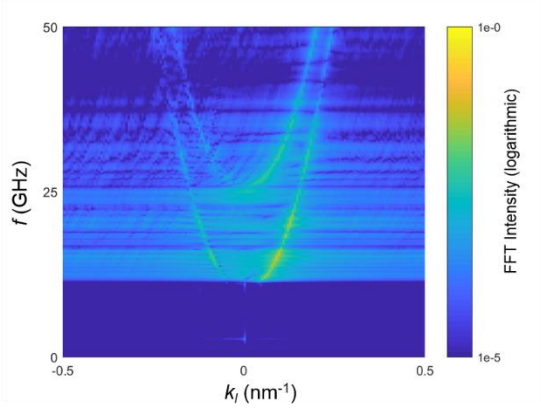

(c)

Figure 3.3 The dispersion curve in (a) inlet MNW (red circle: primary concave, green circle: secondary concave, blue: flat branches), (b) outlet MNW 1, (c) outlet MNW 2

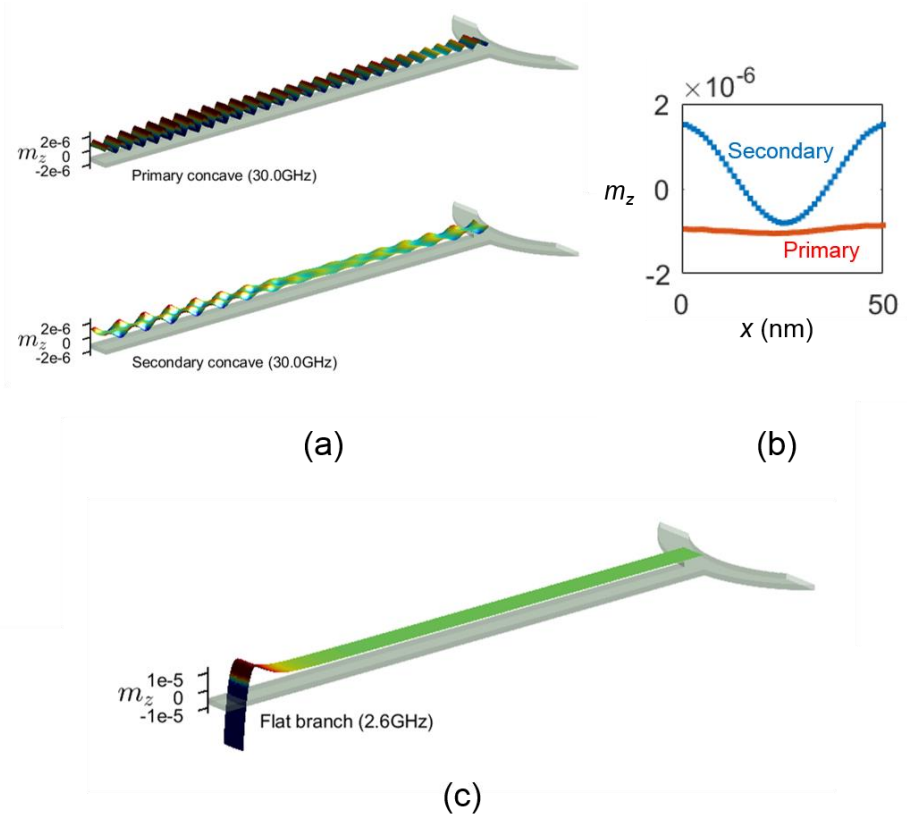

Figure 3.4 (a) Inverse Fourier transform at 30.0 GHz on both concaves and (b) their width profile, (c) inverse Fourier transform at 2.6 GHz

3.3. Spin-wave duplex in model system A and B

After the spin-waves travel through all the segments, the resultant spin-wave amplitude in both outlet MNWs should show the signal transmission behavior similar to that of the duplexer: the signal entered in one MNW should be sent to the neighboring MNW, and the signal entered in this MNW should be sent to the next neighboring MNW. The mode spectra in outlet MNWs were averaged in the longitudinal direction (Figure 3.5 (a), (b1), (b2), (b3)), showing that in model system A, the spin-wave entering any MNWs will be sent to the other MNWs evenly.

However, in model system B, the spin-wave may show the signal transmission akin to that of duplexer at some frequencies. For example, from the Figure 3.5 (b1)-(b3), in model system B, the 13.8 GHz signal is sent from top-left MNW to the bottom MNW, and the 15.0 GHz signal is sent from bottom MNW to the top-right MNW. The signal transmissions at 13.8 GHz and 15.0 GHz are summarized in the corresponding inverse Fourier transform data over the whole system (Figure 3.6).

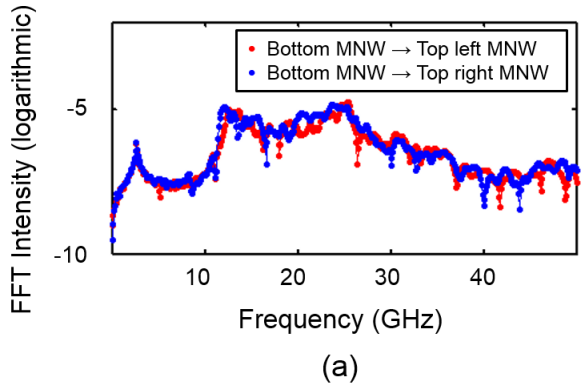

(a)

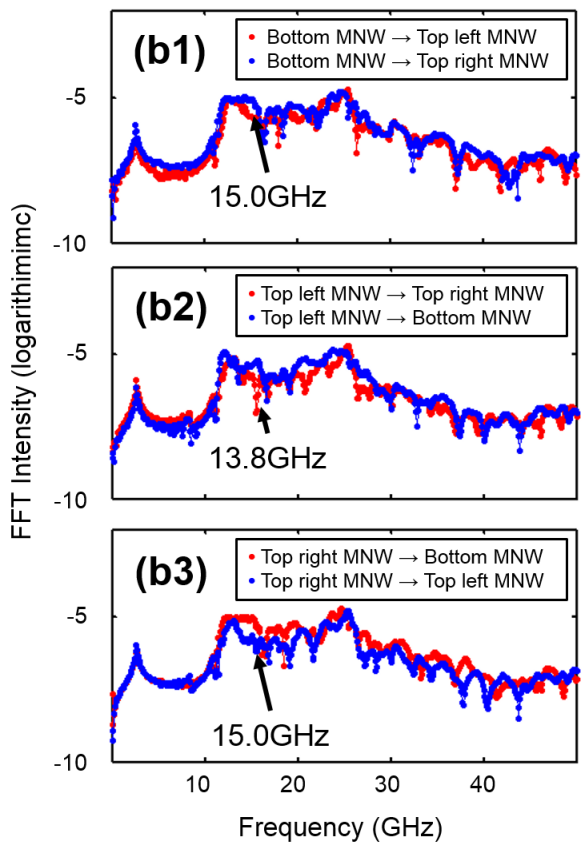

(b)

Figure 3.5 The average mode spectra along the longitudinal direction, which summarized the spin-wave propagation inside (a) spin-wave system A, (b1-3) spin-wave system B

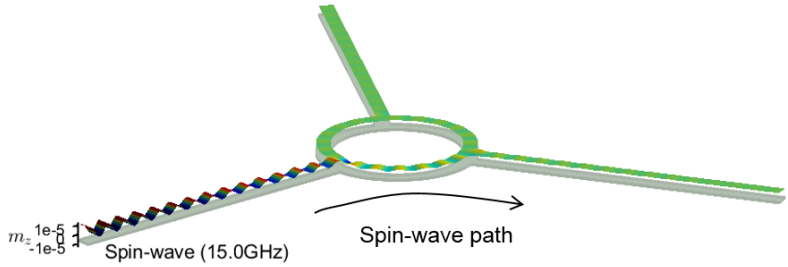

(a)

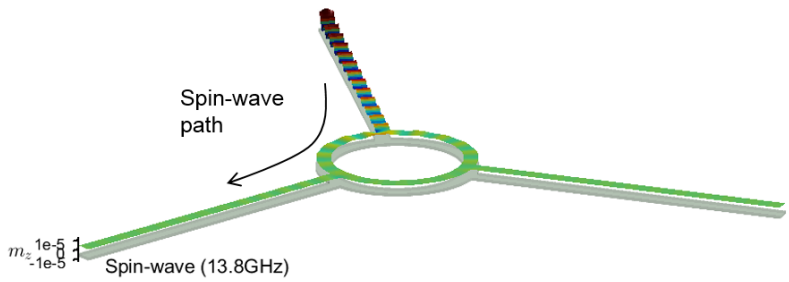

(b)

Figure 3.6 Inverse Fourier transform for (a) 15.0 GHz spin-wave entering from bottom MNW, (b) 13.8 GHz spin-wave entering from top-left MNW

Chapter 4. Conclusion

In this thesis the model system of spin-wave duplexer which is composed of three magnetic nanowires (MNWs) and the ring is proposed and studied with micromagnetics simulation. The model is made of Permalloy and may have 16 spin configurations, but according to the LLG equation which governs the micromagnetics simulation, it is expected that the simulation in two spin configurations is enough to cover all other possibilities of spin configuration. The spin-wave propagation behavior in the proposed model can be simulated by exciting spin-wave at each end of the MNWs, and it turns out that the signal transport behavior similar to duplexer is displayed in one of the two spin configurations. In the spin configuration, halfvortices which are barely visited topological defect are asymmetrically distributed, and the combined effect of nonuniform magnetization and nonuniform effective field, and abrupt change in wave vector direction leads to the deflection of propagating spin-waves.

As one of the derivatives of the three-port circulator, which have gained lots of attentions recently with regard to its miniaturization, the spin-wave duplexer, when realized, would mark one step forward to the relevant studies.

Bibliography

1. H. John Caulfield and Shlomi Dolev, “Why future supercomputing requires optics”, *Nature Photonics* **4**, 261-263 (2010).
2. Wang, L. and Li, B., “Thermal logic gates: computation with phonons”, *Phys. Rev. Lett.* **99**, 177208 (2007).
3. Pavel Kabos and V.S. Stalmachov, “Magnetostatic Waves and Their Application”, Springer Science & Business Media (2012).
4. Wolf, S. A. *et al.*, “Spintronics: a spin-based electronics vision for the future”, *Science* **294**, 1488-1495 (2001).
5. Khitun, A., Ostroumov, R. and Wang, K. L. “Spin-wave utilization in a quantum computer”, *Phys. Rev. A* **64**, 062304 (2001).
6. Behin-Aein, B., Salahuddin, S. and Datta, S., “Switching energy of ferromagnetic logic bits”, *IEEE Trans. Nanotech.* **8**, 505-514 (2009).
7. Bandyopadhyay, S. and Cahay, M, “Electron spin for classical information processing: a brief survey of spin-based logic devices, gates and circuits”, *Nanotechnology* **20**, 412001 (2009).
8. Walker, L. R., “Magnetostatic modes in ferromagnetic resonance”, *Phys. Rev.* **105**, 390-399 (1957).
9. Bailleul, M., Olligs, D. and Fermon, C., “Propagating spin wave spectroscopy in a permalloy film: A quantitative

analysis", *Appl. Phys. Lett.* **83**, 972-974 (2003).

10. F. Bertaut and F. Forrat, "Structure des ferrites ferrimagnétiques des terres rares", *C. R. Acad. Sci. Paris* **242**, 382–384 (1956).
11. R. C. Fletcher, R. C. LeCraw, and E. G. Spencer, "Electron Spin Relaxation in Ferromagnetic Insulators", *Phys. Rev.* **117**, 955 (1960).
12. Martin A. W. Schoen, Danny Thonig, Michael L. Schneider, T. J. Silva, Hans T. Nembach, Olle Eriksson, Olof Karis and Justin M. Shaw, "Ultra-low magnetic damping of a metallic ferromagnet", *Nature Physics* **12**, 839–842 (2016).
13. William Fuller Brown, Jr, "Micromagnetics : Successor to Domain Theory?", *LE JOURNAL DE PHYSIQUE ET LE RADIUM* **20**, 101-104 (1959).
14. Yoshinobu Nakatani, Yasutaro Uesaka and Nobuo Hayashi, "Direct Solution of the Landau-Lifshitz-Gilbert Equation for Micromagnetics", *Japanese Journal of Applied Physics* **28**, 12 (1989).
15. Werner Scholz, Josef Fidler, Thomas Schrefl, Dieter Suess, Rok Dittrich, Hermann Forster, Vassilios Tsiantos, "Scalable Parallel Micromagnetic Solvers for Magnetic Nanostructures", *Computational Materials Science* **28**, 366-383 (2003).
16. G. Srinivasan and C. E. Patton, "Direct detection of magnetostatic wave excitations in magnetostatic wave device structures by Brillouin light scattering", *Appl. Phys. Lett.* **47**,

759 (1985).

17. O. Klein, V. Charbois, V. V. Naletov, and C. Fermon, “Measurement of the ferromagnetic relaxation in a micron-size sample”, *Phys. Rev. B* **67**, 220407(R) (2003).
18. Oleg Tchernyshyov and Gia-Wei Chern, “Fractional Vortices and Composite Domain Walls in Flat Nanomagnets”, *Phys. Rev. Lett.* **95**, 197204 (2005).
19. Keisuke Yamada, Shinya Kasai, Yoshinobu Nakatani, Kensuke Kobayashi, Hiroshi Kohno, André Thiaville and Teruo Ono, “Electrical switching of the vortex core in a magnetic disk”, *Nature Materials* **6**, 270-273 (2007).
20. B. Van Waeyenberge, A. Puzic, H. Stoll, K. W. Chou, T. Tyliszczak, R. Hertel, M. Fähnle, H. Brückl, K. Rott, G. Reiss, I. Neudecker, D. Weiss, C. H. Back and G. Schütz, “Magnetic vortex core reversal by excitation with short bursts of an alternating field”, *Nature* **444**, 461-464 (2006).
21. B. Pigeau, G. de Loubens, O. Klein, A. Riegler, F. Lochner, G. Schmidt, L. W. Molenkamp, V. S. Tiberkevich, and A. N. Slavin, “A frequency-controlled magnetic vortex memory”, *Appl. Phys. Lett.* **96**, 132506 (2010).
22. K. Nakano, D. Chiba, N. Ohshima, S. Kasai, T. Sato, Y. Nakatani, K. Sekiguchi, K. Kobayashi, and T. Ono, “All-electrical operation of magnetic vortex core memory cell”, *Appl. Phys. Lett.* **99**, 262505 (2011).
23. Z. Li and S. Zhang, “Domain-Wall Dynamics and Spin-Wave Excitations with Spin-Transfer Torques”, *Phys. Rev.*

Lett. **92**, 207203 (2004).

24. P. Yan, X. S. Wang, and X. R. Wang, "All-Magnonic Spin-Transfer Torque and Domain Wall Propagation", *Phys. Rev. Lett.* **107**, 177207 (2011).
25. J. P. Park and P. A. Crowell, "Interactions of Spin Waves with a Magnetic Vortex", *Phys. Rev. Lett.* **95**, 167201 (2005).
26. V. L. Carvalho-Santos, R. G. Elías and A. S. Nunez, "Spin wave vortex from the scattering on Bloch point solitons", *Annals of Physics* **363**, 364-370 (2015).
27. Junichi Iwasaki, Aron J. Beekman, and Naoto Nagaosa, "Theory of magnon-skyrmion scattering in chiral magnets", *Phys. Rev. B* **89**, 064412 (2014).
28. Christoph Schütte and Markus Garst, "Magnon-skyrmion scattering in chiral magnets", *Phys. Rev. B* **90**, 094423 (2014).
29. N. D. Mermin, "The topological theory of defects in ordered media", *Rev. Mod. Phys.* **51**, 591 (1979).
30. Sinead M. Griffin and Nicola A. Spaldin, "On the relationship between topological and geometric defects", arXiv:1703.05225v1 [cond-mat.mtrl-sci].
31. J. Rothman, M. Kläui, L. Lopez-Diaz, C. A. F. Vaz, A. Bleloch, J. A. C. Bland, Z. Cui, and R. Speaks, "Observation of a Bi-Domain State and Nucleation Free Switching in Mesoscopic Ring Magnets", *Phys. Rev. Lett.* **86**, 1098 (2001).
32. Kibble, T. W. B. "Topology of cosmic strings and domains",

J. Phys. A: Math. Gen. **9**, 1387 (1976).

33. J. M. Carlson, S. A. Langer and J. P. Sethn, “Frustration in Modulated Phases: Ripples and Boojums”, *Europhys. Lett.* **5**, 327-331 (1988).
34. Aakash Pushp, Timothy Phung, Charles Rettner, Brian P. Hughes, See-Hun Yang, Luc Thomas, Stuart S. P. Parkin, “Domain wall trajectory determined by its fractional topological edge defects”, *Nature Physics* **9**, 505–511 (2013).
35. Jun-Young Lee, Ki-Suk Lee, Sangkook Choi, Konstantin Y. Guslienko, and Sang-Koog Kim, “Dynamic transformations of the internal structure of a moving domain wall in magnetic nanostripes”, *Phys. Rev. B* **76**, 184408 (2007).
36. B. A. Kalinikos and A. N. Slavin, “Theory of dipole-exchange spin wave spectrum for ferromagnetic films with mixed exchange boundary conditions”, *Journal of Physics C: Solid State Physics* **19**, 35 (1986).
37. Dae-Eun Jeong, Dong-Soo Han and Sang-Koog Kim, “Refractive Index and Snell’s Law for Dipole-exchange Spin Waves in Restricted Geometry, *SPIN* **1**, 1 (2011).
38. J. Stigloher, M. Decker, H. S. Körner, K. Tanabe, T. Moriyama, T. Taniguchi, H. Hata, M. Madami, G. Gubbiotti, K. Kobayashi, T. Ono, and C. H. Back, “Snell’s Law for Spin Waves”, *Phys. Rev. Lett.* **117**, 037204 (2016).
39. C. S. Davies, A. Francis, A. V. Sadovnikov, S. V. Chertopalov, M. T. Bryan, S. V. Grishin, D. A. Allwood, Y. P.

Sharaevskii, S. A. Nikitov and V. V. Kruglyak, “Towards graded-index magnonics: Steering spin waves in magnonic networks”, *Phys. Rev. B* **92**, 020408(R) (2015).

40. S. O. Demokritov, A. A. Serga, A. Andre, V. E. Demidov, M. P. Kostylev, and B. Hillebrands, “Tunneling of Dipolar Spin Waves through a Region of Inhomogeneous Magnetic Field”, *Phys. Rev. Lett.* **93**, 4 (2004).
41. A. V. Sadovnikov, C. S. Davies, S. V. Grishin, V. V. Kruglyak, D. V. Romanenko, Yu. P. Sharaevskii, and S. A. Nikitov, “Magnonic beam splitter: The building block of parallel magnonic circuitry”, *Applied Physics Letters* **106**, 192406 (2015).
42. P. Gruszecki, J. Romero-Vivas, Yu. S. Dadoenkova, N. N. Dadoenkova, I. L. Lyubchanskii, and M. Krawczyk, “Goos-Hänchen effect and bending of spin wave beams in thin magnetic films”, *Applied Physics Letters* **105**, 242406 (2014).
43. S. V. Vasilieva, V. V. Kruglyakb, M. L. Sokolovskiic, and A. N. Kuchkod, “Spin wave interferometer employing a local nonuniformity of the effective magnetic field”, *Journal of Applied Physics* **101**, 113919 (2007).
44. P. Clausen, K. Vogt, H. Schultheiss, S. Schäfer, B. Obry, “Mode conversion by symmetry breaking of propagating spin waves”, *Appl. Phys. Lett*. **99**, 162505 (2011).
45. A. V. Chumak, A. A. Serga, S. Wolff, B. Hillebrands, and M. P. Kostylev, “Scattering of surface and volume spin waves in

a magnonic crystal", *Appl. Phys. Lett.* **94**, 172511 (2009).

46. Xiangjun Xing, Yongli Yu, Shuwei Li and Xiaohong Huang, "How do spin waves pass through a bend?", *Scientific Reports* **3**, 2958 (2013).
47. Xiangjun Xing, Qingli Jin and Shuwei Li, "Frequency-selective manipulation of spin waves: micromagnetic texture as amplitude valve and mode modulator", *New Journal of Physics* **17** (2015).
48. Carlos J. García-Cervera, "Numerical Micromagnetics: A Review", *Bol. Soc. Esp. Mat. Apl. SeMA* **39**, 103–135 (2007).
49. M. Lakshmanan and K. Nakamura, "Landau-Lifshitz Equation of Ferromagnetism: Exact Treatment of the Gilbert Damping", *Phys. Rev. Lett.* **53**, 2497 (1984).
50. V. K. Dugaev, P. Bruno, B. Canals, and C. Lacroix, "Berry phase of magnons in textured ferromagnets", *Physical Review B* **72**, 024456 (2005).
51. Jin Lan (兰金), Weichao Yu (余伟超), Ruqian Wu, and Jiang Xiao (萧江), "Spin-Wave Diode", *Phys. Rev. X* **5**, 041049 (2015).
52. Weichao Yu (余伟超), Jin Lan (兰金), Ruqian Wu, and Jiang Xiao (萧江), "Magnetic Snell's law and spin-wave fiber with Dzyaloshinskii-Moriya interaction", *Phys. Rev. B* **94**, 140410(R) (2016).
53. Riccardo Hertel, Wulf Wulfhekel, and Jürgen Kirschner,

"Domain-Wall Induced Phase Shifts in Spin Waves", *Phys. Rev. Lett*. **93**, 257202 (2004).

54. Shufeng Zhang and Steven S.-L. Zhang, "Generalization of the Landau-Lifshitz-Gilbert Equation for Conducting Ferromagnet", *Phys. Rev. Lett.* **102**, 086601 (2009).
55. Kazushige Hyodo, Chiharu Mitsumata, and Akimasa Sakuma, "Effect of Spin Torque on Magnetization Switching Speed Having Nonuniform Spin Distribution", *IEEE Trans. Magn.* **48**, 11 (2012).
56. Dong-Soo Han, Sang-Koog Kim, Jun-Young Lee, Sebastian J. Hermsdoerfer, Helmut Schultheiss, "Magnetic domain-wall motion by propagating spin waves", *Appl. Phys. Lett.* **94**, 112502 (2009).
57. Soo-Man Seo, Hyun-Woo Lee, Hiroshi Kohno, and Kyung-Jin Lee, "Magnetic vortex wall motion driven by spin waves", *Applied Physics Letters* **98**, 012514 (2011).
58. S. Mamica, "Vortices in two-dimensional nanorings studied by means of the dynamical matrix method", *Low Temperature Physics* **41**, 806 (2015).
59. M. Krawczyk and H. Puszkarski, "Plane-wave theory of three-dimensional magnonic crystals", *Phys. Rev. B* **77**, 054437 (2008).
60. Carlos J. García-Cervera, Zydrunas Gimbutas, Weinan E., "Accurate numerical methods for micromagnetics simulations with general geometries", *Journal of Computational Physics* **184**, 1, (2003).

61. Claas Abert, Lukas Exl, Florian Bruckner, André Drews, Dieter Suess, “magnum.fe: A micromagnetic finite-element simulation code based on FEniCS”, *Journal of Magnetism and Magnetic Materials* **345**, 29-35 (2013).
62. D. R. Fredkin, T.R. Koehler, “Hybrid method for computing demagnetizing fields”, *IEEE Transactions on Magnetics* **26**, 2 (1990).
63. Qiushi Chen, “A Review of Finite Element Open Boundary Techniques for Static and Quasi-Static Electromagnetic Field Problems”, *IEEE Trans. Magn.* **33**, 1 (1997).
64. A. Khebir, A.B. Kouki, R. Mittra, “Asymptotic boundary conditions for finite element analysis of three-dimensional transmission line discontinuities”, *IEEE Transactions on Microwave Theory and Techniques* **38**, 10 (1990).
65. X. Brunotte, G. Meunier and J.F. Imhoff, “Finite element modelling of unbounded problems using transformations: rigorous, powerful and easy solutions”, *IEEE Transactions on Magnetics* **28**, 1663 (1992).
66. Konstantin Y. Guslienko, Andrei N. Slavin, “Magnetostatic Green's functions for the description of spin waves in finite rectangular magnetic dots and stripes”, *Journal of Magnetism and Magnetic Materials* **323**, 2418-2424 (2011).
67. R. Zivieri and R. L. Stamps, “Theory of spin wave modes in tangentially magnetized thin cylindrical dots: A variational approach”, *Phys. Rev. B* **73**, 144422 (2006).
68. Nobuo Hayashi, Koji Saito and Yoshinobu Nakatani,

"Calculation of Demagnetizing Field Distribution Based on Fast Fourier Transform of Convolution", *Japanese Journal of Applied Physics* **35**, 12A (1996).

69. Alexander Baker, Marijan Beg, Gregory Ashton, Maximilian Albert, Dmitri Chernyshenko, Weiwei Wang, Shilei Zhang, Marc-Antonio Bisotti, Matteo Franchin, Chun Lian Hud, Robert Stamps, Thorsten Hesjedal, Hans Fangohr, "Proposal of a micromagnetic standard problem for ferromagnetic resonance simulations", *Journal of Magnetism and Magnetic Materials* **421**, 428-439 (2017).
70. R.D. McMichael, M.D. Stiles, "Magnetic normal modes of nanoelements", *J. Appl.Phys.* **97** 10J901 (2005).
71. Peter J. Metaxas, Maximilian Albert, Steven Lequeux, Vincent Cros, Julie Grollier, Paolo Bortolotti, Abdelmadjid Anane, and Hans Fangohr, "Resonant translational, breathing, and twisting modes of transverse magnetic domain walls pinned at notches", *Phys. Rev. B* **93**, 054414 (2016).
72. D.V. Berkov, "Numerical simulations of quasistatic remagnetization processes infine magnetic particle systems", *Journal of Magnetism and Magnetic Materials* **161** 337-356 (1996).
73. Gia-Wei Chern, David Clarke, Hyun Youk, and Oleg Tchernyshyov, "Halfvortices in flat nanomagnets", arXiv:1007.2158v1 [cond-mat.mtrl-sci]
74. Manfred E. Schabes, "Micromagnetic theory of non-uniform

magnetization processesin magnetic recording particles", *Journal of Magnetism and Magnetic Materials* **95**, 249-288 (1991).

75. M.J.Donahue and R.D.McMichael, "Exchange energy representations in computational micromagnetics", *Physica B: Condensed Matter* **233**, 4 (1997).
76. T. Devolder, J.-V. Kim, L. Nistor, R. Sousa, B. Rodmacq, and B. Dieny, "Exchange stiffness in ultrathin perpendicularly-magnetized CoFeB layers determined using spin wave spectroscopy", *Journal of Applied Physics* **120**, 183902 (2016).
77. G. Venkat, H. Fangohr, A. Prabhakara, "Absorbing boundary layers for spin wave micromagnetics", arXiv:1706.03325v1 [cond-mat.mes-hall].
78. Sangkook Choi, Ki-Suk Lee, Konstantin Yu. Guslienko, and Sang-Koog Kim, "Strong Radiation of Spin Waves by Core Reversal of a Magnetic Vortex and Their Wave Behaviors in Magnetic Nanowire Waveguides", *Phys. Rev. Lett.* **98**, 087205 (2007).
79. K. Yu. Guslienko and A. N. Slavin, "Boundary conditions for magnetization in magnetic nanoelements", *Phys. Rev. B* **72**, 014463 (2005).
80. Wenjun Dong, Yuanchang Su, Haiyang Lei, and Jingguo Hu. "Manipulation of multiple 360^{o} domain wall structures and its current-driven motion in a magnetic nanostripe", *AIP Advances* **5**, 117215 (2015).

81. RFDH, “RF 기초강의실”, 코너북 (2016).
82. 이기복, “초단파용 송수 분리기(Duplexer) 필터의 설계에 관한 연구” (1996), 동아대학교 대학원 학위논문.
83. 최정훈, “ZnO 압전박막을 이용한 SAW Duplexer 제조 및 특성” (2004), 연세대학교 대학원 학위논문.
84. 윤석출, “휴대폰용 FBAR Duplexer에 내장되는 위상천이기에 관한 연구” (2004), 한밭대학교 대학원 학위논문.
85. Giovanni Viola and David P. DiVincenzo, “Hall Effect Gyrators and Circulators”, *Phys. Rev. X* **4**, 021019 (2014).
86. N. Roch *et al.*, “Observation of measurement-induced entanglement and quantum trajectories of remote superconducting qubits”, arXiv:1402.1868v2 [cond-mat.mes-hall]
87. Baleegh Abdo *et al.*, “Directional Amplification with a Josephson Circuit”, *Phys. Rev. X* **3**, 031001 (2013).
88. Jens Koch *et al.*, “Time-reversal-symmetry breaking in circuit-QED-based photon lattices”, *Phys. Rev. A* **82**, 043811 (2010).
89. Sangkook Choi, Ki-Suk Lee, Konstantin Yu. Guslienko, and Sang-Koog Kim, “Strong Radiation of Spin Waves by Core Reversal of a Magnetic Vortex and Their Wave Behaviors in Magnetic Nanowire Waveguides”, *Phys. Rev. Lett.* **98**, 087205 (2007).

90. K. Yu. Guslienko, S. O. Demokritov, B. Hillebrands, and A. N. Slavin, “Effective dipolar boundary conditions for dynamic magnetization in thin magnetic stripes”, *Phys. Rev. B* **66**, 132402 (2002).
91. K. Vogt, F.Y. Fradin, J.E. Pearson, T. Sebastian, S.D. Bader, B. Hillebrands, A. Hoffmann & H. Schultheiss, “Realization of a spin-wave multiplexer”, *Nature Communications* **5**, 3727 (2014).
92. Xiangjun Xing, Philip W. T. Pong, J. Åkerman, and Yan Zhou, “Paving Spin-Wave Fibers in Magnonic Nanocircuits Using Spin-Orbit Torque”, *Phys. Rev. Applied* **7**, 054016 (2017).
93. Manfred E. Schabes, “Micromagnetic theory of non-uniform magnetization processes in magnetic recording particles”, *Journal of Magnetism and Magnetic Materials* **95**, 249-288 (1991).

Abstract

듀플렉서는 송/수신자 사이의 쌍방향 통신을 위한 전자소자로 최근 소형화에 대한 연구가 진행 중인 써큘레이터로부터 파생되는 소자이다. 최근에 알려진 스핀파는 GHz대의 가동 주파수와 줄열이 아닌 에너지 손실 메커니즘을 가진 정보 전달 매체이나, 스핀파 회로를 제작한다면 회로 물질의 물성상의 불균일함과 스핀파 파수벡터의 잦은 변화가 스핀파의 진행 경로를 예측하기 어렵게 만든다는 문제가 있다. 아래 연구에서는 스핀파 듀플렉서의 모델 구조가 제안되고 이미 많은 스핀파 연구에서 스핀동역학의 사실적인 모델링을 제공해온 미소자기전산모사를 통해 연구된다. 제안되는 모델 구조에서는 하프보텍스라 불리는 위상학적 구조가 존재하여 스핀파의 진행 경로가 원활하고 재현 가능한 양상으로 제어될 수 있다.